JOURNAL OF AGRICULTURAL AND FOOD CHEMISTRY

Interaction between Morin and Sodium Dodecyl Sulfate (SDS) Micelles

WEIYA LIU† AND RONG GUO*,‡

Key Laboratory of Mesoscopic Chemistry, Ministry of Education, Department of Chemistry, Nanjing University, Nanjing 210093, People's Republic of China, and School of Chemistry and Chemical Engineering, Yangzhou University, Yangzhou 225002, People's Republic of China

Electronic absorption spectra, fluorescence emission spectra, ATR-FTIR spectra, cyclic voltammetric measurements, and ab initio quantum calculation are used to study the properties of morin in SDS micelles of different microstructures and microenvironments and to gain the information about the binding of morin with the SDS micelles. Morin can be located in the SDS micelles with its phenyl group (deviating by 38.98° from the planarity), which leads to the increase of the planarity and the extension of π conjugation of the whole molecule. The embedment of two hydroxyl groups on the phenyl into a more hydrophobic microenvironment makes the oxidation peak of morin move to a higher potential with a decreased peak current. The binding constant (K) and the distribution coefficient (P) of morin in the spherical SDS micelle are larger than those in the rodlike SDS micelle. The binding of morin with SDS micelle is a spontaneous ($\Delta G < 0$) and exothermic process ($\Delta H < 0$), and the hydrophobic force is the main driving force for its solubilization.

KEYWORDS: Morin; SDS micelle; binding constant; distribution coefficient; micropolarity; cyclic voltammetry

INTRODUCTION

Flavonoids, a group of more than 4000 polyhydroxyphenolic products, are widely distributed in fruits and vegetables (*1*−*5*). Besides their important biological roles in plant pigmentation, nitrogen fixation, and chemical defense, flavonoids possess antiallergic, antiplatelet, antiviral, anticancer, and anti-inflammatory properties and possibly even possess protective effects against chronic diseases (*6*−*9*), which are the consequence of their affinity to proteins (including enzymes) and their antioxidant properties.

Morin (3,2′,4′,5,7-pentahydroxyflavone) (**Figure 1**) is one of the most common flavonols present in nature and has attracted the attention of many researchers because of its biological and pharmaceutical properties (*10*−*12*). Morin may act as antioxidant in various ways including direct quenching of the reactive oxygen species, inhibition of enzymes involved in the production of the reactive oxygen species, chelation of low valent metal ions such as Fe^{2+} or Cu^{2+}, and regeneration of membrane-bound antioxidants such as α-tocopherol (*13*−*15*). However, the solubility of morin in water, which is in the micromolar range, may be too low to protect physiological species effectively from free radical damage, and its polyphenol structure makes it very sensitive to changes in its structure and the polarity of the environment. Accordingly, the antioxidant property of morin varies dramatically with the change of the environment.

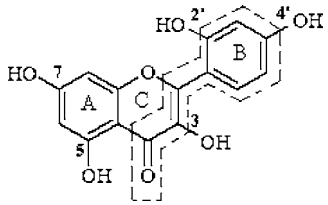

Figure 1. Structure of morin.

The purpose of this investigation was to gain a deeper insight into the structural and electronic properties of morin in the organized sodium dodecyl sulfate (SDS), which not only can solubilize morin to increase its solubility and concentration in the aqueous solution but also can influence the antioxidant ability of the morin greatly with its diversification in structure and microenvironment.

MATERIALS AND METHODS

Chemicals. Morin (99%) was obtained from Merck (Darmstadt, Germany). SDS and pyrene were purchased from Sigma-Aldrich Chemical Co. (St. Louis, MO). The water used was double distilled, and the other chemicals were of analytical reagent grade.

Ab Initio Quantum Calculation. Ab initio quantum calculations of morin were carried out at the level of B3lyp/6-311+g(2d, p)//B3lyp/6-31+g(d, p) with the Gaussian 98 program.

UV−Vis Spectra Measurements. Morin was dissolved in the SDS micelles, and after 1 h of mixing, the spectra were recorded by using a UV-240 spectrophotometer (Shimadzu) in the wavelength range of 200−500 nm. Distilled water was used as blank.

* Author to whom correspondence should be addressed (e-mail guorong@yzu.edu.cn).
† Nanjing University.
‡ Yangzhou University.

10.1021/jf047847p CCC: $30.25
Published on Web 03/26/2005

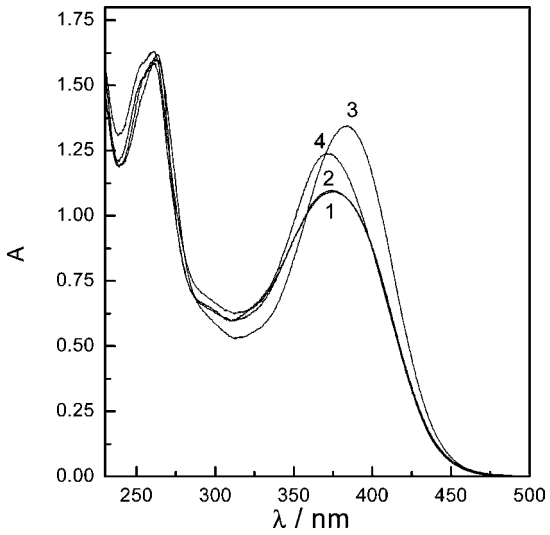

Figure 2. Absorption spectra of morin (1.0×10^{-4} mol/L) in different SDS micelles. SDS: (1) 0.0, (2) 1.0×10^{-4}, (3) 8.0×10^{-3}, and (4) 8.0×10^{-2} mol/L.

ATR-FTIR Spectral Measurements. FTIR spectra of morin in the SDS micelles were recorded with a Brucker Equinox 55 FT-IR spectrometer. Single-beam IR spectra were the result of ~64 co-added interferograms and ranged from 400 to 2000 cm^{-1}, with a spectral resolution of 4 cm^{-1}. A ZnSe ATR optical accessory set at 45° was used as a reflectance medium.

Fluorescence Spectral Measurements. The fluorescence spectra of morin were recorded with an RF-5301 PC spectrofluorophotometer (Shimadzu) in the wavelength range of 400−600 nm with the excitation wavelength being 370 nm. The emission intensities of the polarized light, parallel and vertical to the excitation-polarized light, $I_{\parallel}$ and $I_{\perp}$, were combined to give the following equation of steady-state polarization P:

$$P = (I_{\parallel} - I_{\perp})/(I_{\parallel} + I_{\perp})$$

Measurement of Microenvironment Polarity. Pyrene, used as probe, was dissolved in SDS/morin mixed solution. Its fluorescence spectra show five emission peaks when it was excited at 338 nm. The intensity ratio of the first (at ~373 nm) and the third peaks (at ~384 nm) can show the polarity of the probe microenvironment. Furthermore, the location of morin in the SDS micelles can be determined from the variety of I_1/I_3 values (*16*, *17*).

Determination of Voltammetric Properties of Morin. Cyclic voltammetric experiments were carried out with a CH Instruments 660a electrochemical workstation (Zhenghua, Shanghai, China). Glassy carbon was used as working electrode (3.0 mm diameter), platinum as auxiliary electrode, and saturated calomel as reference electrode. The solutions were prepared in acetic acid−sodium acetate buffers, and the pH values of the system were determined by a PHs-25 PH-meter (Leizi Instrumental Factory, Shanghai, China).

RESULTS AND DISCUSSION

Absorption spectra of morin in different SDS micelles are shown in **Figure 2**. In the range of 240−500 nm, morin exhibits two main absorption bands, referred to as band I (300−400 nm) and band II (240−280 nm) (curve 1 in **Figure 2**) (*18*). Band I is supposed to be associated with the light absorption of the cinnamyl system (the dashed-frame part of the morin molecule in **Figure 1**) and band II with the absorption of the benzoyl moiety (**Figure 1**). These two transitions are $\pi-\pi^*$ in nature and can be represented by two resonance structures depicted in **Figure 3**. The zwitterionic or charge-separated forms in **Figure 3** represent the excited states, and both transitions are electronically allowed because of their large ϵ values. The studies

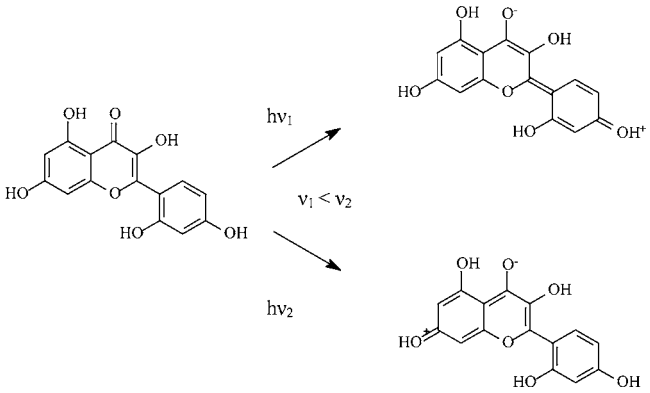

Figure 3. Mesomeric structure illustration of the excited states of morin.

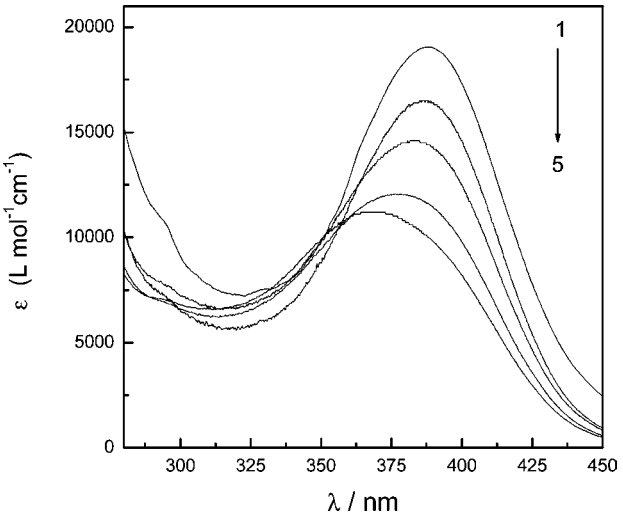

Figure 4. Molar extinction coefficient (ϵ) of morin with wavelength number. Concentration of morin: (1) 1.0×10^{-5}, (2) 2.5×10^{-5}, (3) 4.0×10^{-5}, (4) 7.5×10^{-5}, and (5) 1.0×10^{-4} mol/L.

also show that morin exhibits H aggregation in high concentration (*19*). The relationship between the molar extinction coefficient (ϵ) and wavelength at different concentrations of morin is shown in **Figure 4**. It can be seen from **Figure 4** that the maximum molar extinction coefficient (ϵ_{max}) of morin occurs at 390 nm when the concentration of morin is 10 μmol/L; then, with increasing concentration, the ϵ_{max} undergoes a hipsochromic shift. When the concentration of morin is 0.1 mmol/L, the ϵ_{max} occurs at 370 nm, which means that a morin dimer is formed (*19*). **Figure 2** represents the absorption spectra of morin in the SDS micelles of different structures. The SDS pre-micelle exerts nearly no influence on the morin dimer's absorption spectra (curve 2 in **Figure 2**), the SDS spherical micelle causes a bathochromic shift for band I from 370 to 390 nm and increases the peak intensity (curve 3 in **Figure 2**), whereas the SDS rodlike micelle causes a hipsochromic shift with the absorption peak back to 370 nm and the peak intensity decreased (curve 4 in **Figure 2**). However, no SDS micelles have distinct influence on band II of morin.

As we know, with increasing SDS content, SDS can form pre-micelle (before cmc1), spherical micelle (after cmc1), and rodlike micelle (after cmc2) in the aqueous solution. Morin has aromatic rings, and its solubility in water is low; therefore, morin will be easily extracted into the SDS micelles through hydrophobic interaction. As a result, the solubilizition of morin is inevitably influenced by the different structures and microenvironment of the SDS micelle. When the SDS content is low, it forms pre-micelle in solution. The size and amount of SDS

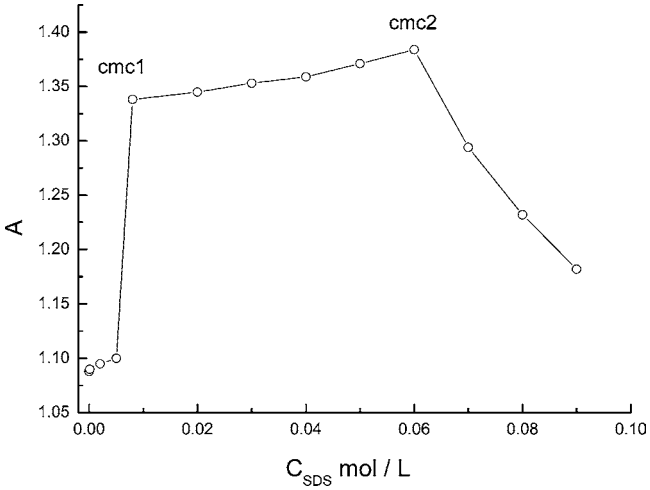

Figure 5. Influence of SDS concentration on the absorbance of morin.

Table 1. Micropolarity of Morin in SDS Micelles

		micropolarity I_1/I_3			
SDS (mol/L)	micelle structure	0×10^{-5} mol/L morin	2.0×10^{-5} mol/L morin	4.0×10^{-5} mol/L morin	6.0×10^{-5} mol/L morin
4.0×10^{-3}	spherical	1.368	1.436	1.543	1.605
8.0×10^{-3}	spherical	1.200	1.239	1.270	1.317
6.0×10^{-2}	rodlike	1.163	1.159	1.140	1.061

pre-micelle are limited, and there exists a static repulsion between SDS and the morin anion (*19*), so the SDS pre-micelle almost has no effect on the morin dimer's absorption spectra. However, the solubilization of morin in the spherical and rodlike SDS micelles alters the aggregation behavior of morin. In the spherical SDS micelle, the morin exists mainly in the form of monomer with the absorption peak at 390 nm; whereas in the rodlike SDS micelle, morin exists mainly in the form of dimer with the absorption peak at 370 nm (**Figure 2**). The different effects of spherical and rodlike SDS micelle on morin can also be seen from **Figure 5**. When the SDS concentration is lower than cmc1, the absorbance of morin exhibits almost no change with SDS concentration; when the SDS concentration arrives at cmc1, the absorbance of morin increases rapidly to a higher value and then remains nearly unchanged; when the SDS concentration is higher than cmc2, the absorbance of morin decreases suddenly. The two inflections on the curve (**Figure 5**) correspond well to the structural change of SDS micelle from spherical to rodlike.

The nanoscale solubilization space provided by SDS micelles is the key factor influencing the aggregation state of the morin. Therefore, we use pyrene as the probe to obtain insight into the microenvironment of the SDS micelle in which morin exists. It is known that the I_1/I_3 of pyrene can be used to measure the environmental polarity (*20*, *21*). From **Table 1**, it can be seen that the values of I_1/I_3 decrease from 1.368 to 1.163 with increasing SDS concentration, which indicates the polarity of the microenvironment for pyrene is decreased with the micelle structure changing from spherical to rodlike. The solubilization of morin into the SDS micelle also leads to the change of the value of I_1/I_3 (**Table 1**). When morin is added to the SDS spherical micelle, the I_1/I_3 values increase; when morin is added to the SDS rodlike micelle, the I_1/I_3 values decrease (**Table 1**). The hydrophobic interaction between morin and the SDS micelle makes morin located in the palisade of the SDS micelle and, thus, changes the location of the pyrene in the SDS micelles.

Table 2. Binding Constant *K* and Distribution Coefficient *P* of Morin in Spherical and Rodlike SDS Micelles

	K		*P*	
morin (10^{-5} mol/L)	spherical micelle	rodlike micelle	spherical micelle	rodlike micelle
1.0	657.3	145.13	2672.95	590.93
2.0	745.0	178.16	3029.46	724.23
3.0	924.4	191.41	3758.72	779.09
4.0	1143.7	222.63	4650.19	906.00
5.0	1214.9	476.5	4939.62	1937.99

The SDS spherical micelle is not so compact and therefore can provide a relatively large solubilization space for morin; once morin is located in SDS spherical micelle, the spaces between SDS molecules are increased and allow the pyrene to be located at the outside of the micellar palisade, so the microenvironment polarity of pyrene is increased. When morin is added to the SDS rodlike micelle, the decreasing solubilization space and the more compact structure no longer permit the pyrene to be locted at the outside of the micellar palisade, and, as a result, pyrene is located in the inner part of the interphase and leads to the decrease of its microenvironmental polarity.

The binding constant (K) of morin with the SDS micelles was obtained by the fluorescence method. The model employed to determine the binding constant between fluorescent molecules and micelles is based on the fluorescence quantum yields in both aqueous and ordered micelles. The binding constant, K, is obtained from the following equation (*22*):

$$\left[\left(\frac{I}{I_0}\right) - 1\right]^{-1} = \left[\left(\frac{I_M}{I_0}\right) - 1\right]^{-1} \times \left[1 + \frac{1}{\gamma K C_S}\right] \quad (1)$$

Here, I is the fluorescence intensity of the system, I_0 is the fluorescence intensity of the system in the absence of micelle, I_M is the maximum fluorescence intensity obtained, C_S is the concentration of the surfactant, and γ is the extinction coefficient ($\gamma = 1$). However, because the increase of morin fluorescence intensity always takes place at a concentration higher than the critical micelle concentration (cmc), the corresponding C_S values must be changed to a micellar form, C_M, expressed by

$$C_M = (C_S - \text{cmc}) \quad (2)$$

Therefore, by substitution of eq 2 into eq 1, an expression that relates the increase of fluorescence intensity with the concentration of micellized surfactant can be obtained:

$$\left[\left(\frac{I}{I_0}\right) - 1\right]^{-1} = \left[\left(\frac{I_M}{I_0}\right) - 1\right]^{-1} \times \left[1 + \frac{1}{\gamma K (C_S - \text{cmc})}\right] \quad (3)$$

The plot of $[(I/I_0) - 1]^{-1}$ versus $1/(C_S - \text{cmc})$ gives a straight line, and the value of the binding constant can be obtained from the quotient of the intercept and slope of this line. The distribution coefficient (P_{MW}) of morin between the SDS micelle phase and the bulk aqueous phase can be obtained through the following equation (*23*):

$$K = (P_{MW} - 1)\bar{V} \quad (4)$$

where K is the binding constant, P_{MW} is the distribution coefficient, and $\bar{V}$ is the partial molar volume ($\bar{V}_{SDS}$ is 0.246L/mol). **Table 2** shows the binding constant K and the distribution coefficient P of morin in spherical and rodlike SDS micelles, respectively. It can be seen from **Table 2** that the

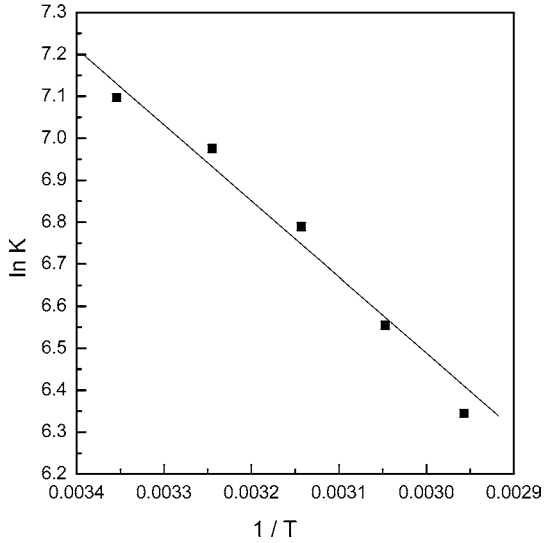

Figure 6. Linear dependence of the ln *K* on 1/*T*.

Table 3. Binding Constant of Morin with SDS Micelles and the Thermodynamic Functions of the Binding Process

T (°C)	morin (10^{-5} mol/L)	*K*	Δ*G* (kJ/mol)	Δ*S* (J/mol·K)	Δ*H* (kJ/mol)
25.0		1143.7	–17.46	8.15	
35.0		1069.3	–17.87	9.21	
45.0	4.0	969.8	–18.19	9.93	–15.03
55.0		702.8	–17.88	8.69	
65.0		568.9	–17.83	8.28	

values of binding constant *K* and the distribution coefficient *P* of morin in the rodlike micelles are much smaller than those in the spherical micelles, which further confirms our above conclusion about the larger solubilization space provided by the spherical SDS micelles. The thermodynamics functions of the binding process can be calculated from the following equations:

$$\Delta G = -RT \ln K_D \tag{5}$$

$$\ln K = -\frac{\Delta H}{R}\left(\frac{1}{T}\right) + C \tag{6}$$

$$\Delta G = \Delta H - T\Delta S \tag{7}$$

Here Δ*G* is the Gibbs free energy, Δ*H* is the enthalpy, *C* is a constant, and *T* is the absolute temperature. The slope of the plot of ln *K* versus 1/*T* can be used to calculate the enthalpy (Δ*H*) (**Figure 6**). From **Table 3**, we can see that the binding of morin to the SDS micelles is a spontaneous behavior (Δ*G* < 0), and the value of Δ*G* becomes more negative with the increase of morin content. Δ*H* < 0, indicating the process of morin solubilization in the SDS micelles is an exothermic process. The rise in the temperature is unfavorable to the location of the morin in the SDS micelle. Thus, the value of *K* decreases with increasing temperature accordingly. In addition, the value of Δ*H* (−15.03 kJ/mol) is smaller than the value of the interaction energy of the chemical bond (>100 kJ/mol) (*21*), indicating the interaction force between morin and SDS micelle is a weak intermolecular force (mainly hydrophobic force).

To make clear which part of the morin molecule can be located in the micelle is also very important, for the location not only changes the electron structure of morin but also alters its aggregation state and antioxidant properties. The $\pi-\pi^*$ excitation of bands I and II of morin involves the π system of

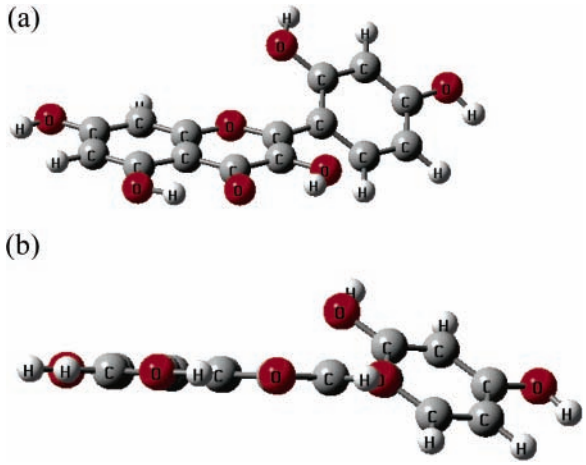

Figure 7. Optimized structure of morin molecule: (**a**) top view; (**b**) side view.

both B- and C-rings and A- and C-rings in the molecule, respectively (**Figure 1**). The ab initio quantum chemical calculations of morin show that the stable structure of morin is not planar, with the B-ring connected to the C-ring by a single C−C bond around which rotation can occur, and the B-ring deviates by 38.98° from planarity (**Figure 7**, from top and side views). Judging from its optimized structure, we deduce that morin is very likely to be located in the SDS micelle with its B-ring part. The changes of the morin absorption spectra in the SDS micelle also confirm that conclusion. Seen from **Figure 2**, almost no SDS micelle can influence the absorption of band II in morin, which means the $\pi-\pi^*$ excitation of band II has not been interrupted; however, the absorption intensity of band I in the SDS spherical and rodlike micelles is greatly increased. As we know, the increase of the molecular planarity of morin and the decrease of the collision frequency of solvent molecules to the morin usually lead to absorption enhancement (*13*). It is reasonable to assume that the location of the dashed-frame part of the morin molecule (**Figure 1**) in the SDS micelle limits the rotation of the C−C single bond linking the B- and C-rings and leads to the increase of the planarity of the whole morin molecule and the extension of π conjugation of the band I of the morin molecule. That is why the absorption intensity of band I is increased greatly in the SDS micelles. In contrast to the case for the dashed-frame part of morin, the SDS micelle does not solubilize the rigid and planar A-ring of the morin; therefore, its π orbital involved in the $\pi-\pi^*$ transitions remains unaltered and the absorption intensity (band II) unchanged (**Figure 2**).

ATR-FTIR spectroscopy has been used to validate the proposed location mechanism. The ATR-FTIR spectra of the free morin and the morin in different SDS micelles are shown in **Figure 8** with the spectra ranging from 1400 to 2200 cm^{-1}, where the very spectra we are interested in appear. For the free morin molecule, the two bands located at 1651 and 1596 cm^{-1} are the stretching vibration of C═O and the phenyl skeleton, respectively (curve 1 in **Figure 8**). The original ν(C═O) band of the free morin is at 1651 cm^{-1}, which is the expectant result of the coupling between C═O and C═C stretching in the morin molecule. The addition of the SDS micelles makes the ν(C═O) band take a shift to a lower frequency (1627 cm^{-1}) with increasing intensity and cover phenyl skeleton stretching vibration at 1596 cm^{-1} and eventually form a broad band centered at 1627 cm^{-1} (curves 2−4 in **Figure 8**). As we know, with the extension of π conjugation and the increase of the planarity of the whole morin molecule, the C═O stretching

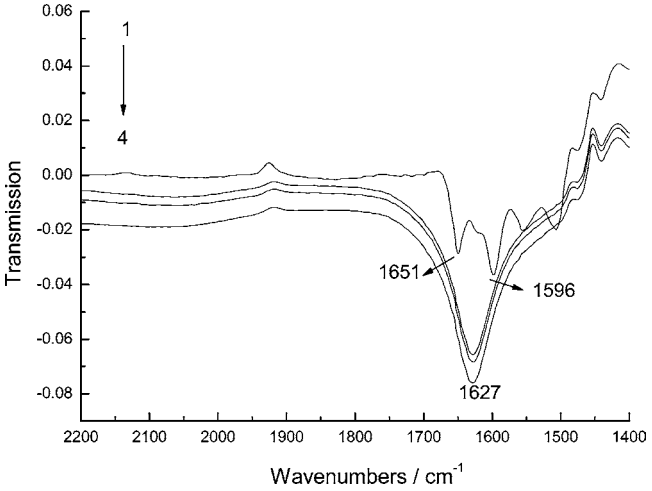

Figure 8. ATR-FTIR spectra of morin (1.0×10^{-2} mol/L) in SDS micelles. SDS: (1) 0.0, (2) 8.0×10^{-3}, (3) 1.0×10^{-2}, and (4) 2.5×10^{-2} mol/L.

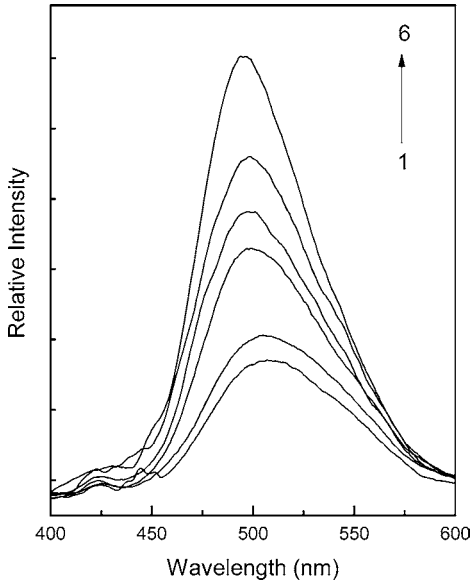

Figure 9. Effect of SDS micelles on fluorescent spectra of morin (1×10^{-4} mol/L). Ex = 370 nm. SDS: (1) 0, (2) 2.0×10^{-3}, (3) 5.0×10^{-3}, (4) 8.0×10^{-3}, (5) 1.0×10^{-2}, amd (6) 2.0×10^{-2} mol/L.

vibration will move to a lower frequency and the band intensity will be greatly enhanced (*24*). The ATR-FTIR spectra observations provide evidence for the location position of morin. With the dashed-frame part of the morin molecule (B-ring) solubilized in the SDS micelle, the rotation of the B-ring is limited and the planarity of the whole molecule is increased, eventually leading to the above change of the molecule vibration in the morin.

The interaction of morin with the SDS micelle is further studied by the fluorescence method. The fluorescence spectra of the morin at ~500 nm when excited at 370 nm can be ascribed to the proton-transfer tautomer fluorescence band ($S_1 \rightarrow S_2$ fluorescence) (**Figure 9**). When morin is mixed with SDS micelles, its relative fluorescence intensity is increased markedly. The plot of the fluorescence polarization (*P*) against the SDS concentration shows two inflections; when the SDS concentration is larger than the first inflection, the values of *P* decrease with the increase of SDS, and when the SDS concentration is larger than the second inflection, the values of *P* show a little increase. These two inflections are very close to cmc1 and cmc2 of the SDS micelles (**Figure 10**), which shows that SDS micelles

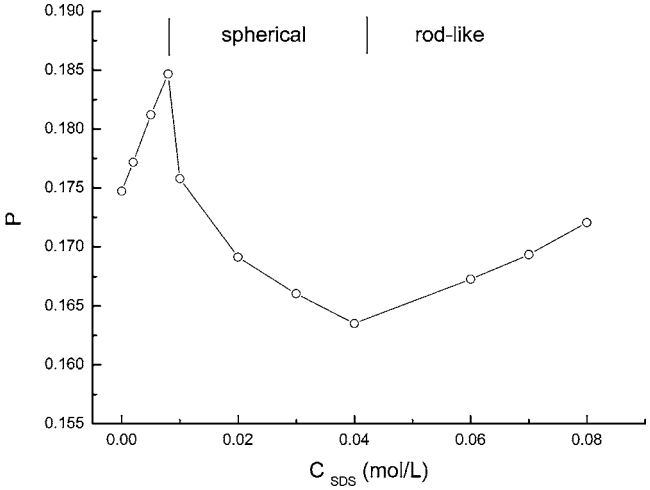

Figure 10. Variation in the fluorescence polarization (*P*) of morin (1×10^{-4} mol/L) with SDS concentration.

with different structures have different effects on the fluorescence polarization of the morin. The enhancement of the proton-transfer tautomer fluorescence of morin by SDS micelles can be rationalized in terms of the interference of the intramolecular hydrogen bonds of morin. It is known that the H-bond between C(4)═O···HO—C(5) will facilitate the nonradiative deactivation, whereas that between C(4)═O···HO—C(3) will permit the ESPT process (*25*, *26*).

With the morin located in the SDS micelle with the dashed-frame part shown in **Figure 1**, the formation of a C(4)═O···HO—C(5) H-bond is restrained because of the exclusion of C(5)—OH outside the micelle, wheres the C(4)═O···HO—C(3) H-bond is enhanced because of the solubilization of both C(4)═O and C(3)—OH in the micelle. That is to say, the nonradiative deactivation process is weakened and the ESPT process is enhanced, so the PT tautomer fluorescence band of the morin is enhanced by the SDS micelles.

As we know, the fluorescence polarization (*P*) has a relationship with the molecular rotation velocity and the microviscosity. The different change tendency of the fluorescence polarization (*P*) of morin with the SDS concentration can also indicate its aggregation state. When morin is mainly in the form of monomer in the SDS spherical micelle, the rotation velocity of the morin molecules is increased and the microviscosity of the system is reduced, so the values of *P* decrease (**Figure 10**). With the formation of the rodlike SDS micelle, morin mainly exists in the form of dimer. The rotation of the morin molecules slows, the microviscosity of the system increases, and the values of the *P* increase with the concentration of SDS rodlike micelles accordingly (**Figure 10**).

Cyclic voltammetry of morin in water and in different SDS micelles has been studied to detect whether the SDS micelle changes the antioxidant activity of the morin or not. The experiments are performed in acetic acid—sodium acetate buffer with weak acidity. Under this condition, morin show an oxidant peak and a reduction (P_a and P_c) (**Figure 11**). The peak currents of morin are linearly dependent on the scan rate, which indicates that the electrode reaction of morin is reversible, with both the reactant and product strongly absorbed on the electrode surface

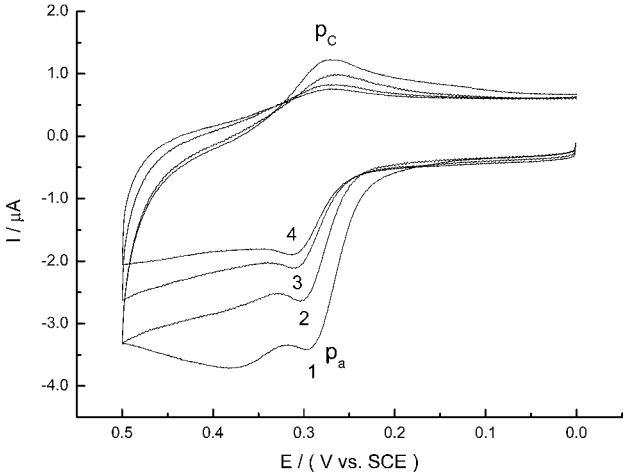

Figure 11. Cyclic voltammograms of morin (4.0×10^{-5} mol/L) mixed with different concentrations of SDS in acetic acid–sodium acetate (0.2 mol/L) buffer with pH being 5.0. SDS: (1) 0.0, (2) 1.0×10^{-4}, (3) 8.0×10^{-3}, and (4) 6.0×10^{-2} mol/L. Scan rate = 200 mV s^{-1}.

(*26*). The peaks correspond to the redox of the 2′,4′-hydroxyl, which is a two-electron and two-proton electrode reaction (*27*).

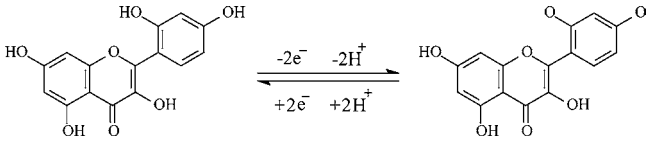

With the addition of the SDS micelle, the oxidant peak of morin moves to a higher potential with lower peak current (**Figure 11**), which means the presence of the SDS micelle makes the oxidation of morin harder. The solubilization of the morin in SDS micelle is the key factor influencing the redox of the morin. With the B-ring part of morin located in the SDS micelle, the electroactive site of morin (2′,4′-hydroxyl) is masked to some extent, which makes the oxidation more difficult and the peak current decrease. The antioxidant and the free radical scavenging capabilities of morin mainly lie in their ability to function as reducing reagent and terminator of radicals by rapid donation of one or two hydrogen atoms to the radicals (*28*). Therefore, whether the location of morin in the SDS micelle and the embedment of the 2′,4′-dihydroxyl group in a more hydrophobic environment change the electrode reaction process tightly linked to the antioxidation capacity of the morin is our special concern. Investigating the variation of the oxidant potential E_{pa} with pH can provide valuable information about the electrode reaction process in which we are interested. It can be seen from **Figure 12** that, with the decrease of the pH values, the oxidation peak of morin shows a higher potential and the peak current is increased. After the addition of SDS micelle, the peak current is decreased and the oxidation peak potential becomes higher, but it seems that the solubilization of morin in the SDS micelle does not alter the change tendency of morin oxidation peak potential with the pH (**Figure 13**). That is to say, the SDS micelle can modulate rather than destroy the redox process of the morin. On the basis of our experimental data, a linear regression equation, $E_{pa} = 0.588 - 0.056$pH (E_{pa}, v; pH, 3.0−6.0; correlation coefficient, $r = 0.997$), of morin is obtained (cruve1, **Figure 13**), which shows that the uptake of electrons is accompanied by an equal number of protons. Whereas in the SDS spherical and rodlike micelles, the linear regressions give $E_{pa} = 0.599 - 0.056$pH (spherical micelle) and $E_{pa} = 0.615 - 0.058$pH (rodlike micelle), respectively (curves 2 and 3, **Figure 13**). The slope of the line shows almost no change compared to that in morin aqueous solution, which means the solubilization of morin in SDS micelle does not change the electrode reaction process of the morin. It is obvious that, with the solubilization of morin in the SDS micelle, the solubility of morin is increased without any destruction of its antioxidant capability.

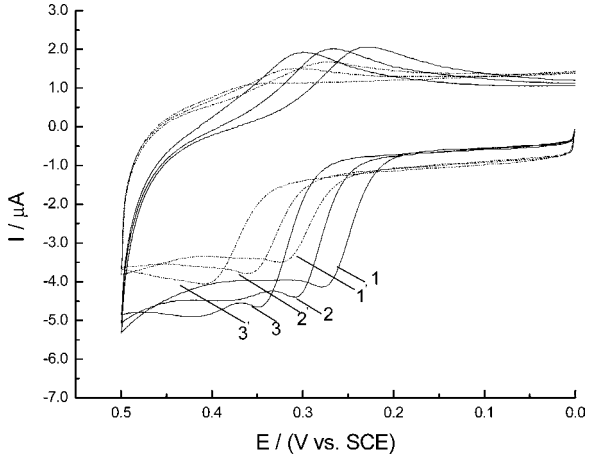

Figure 12. Cyclic voltammograms of morin (4.0×10^{-5} mol/L) in the absence (solid line) and presence (dashed line) of SDS (6.0×10^{-2} mol/L) at various pH values: (1) pH 5.6; (2) pH 5.0; (3) pH 4.4. Scan rate = 200 mV s^{-1}.

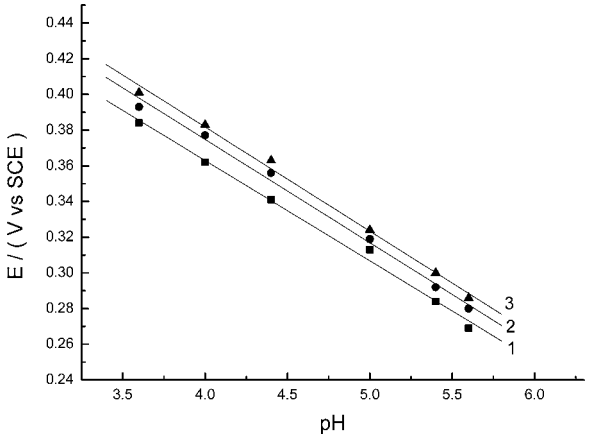

Figure 13. Plot of peak potential (E) of morin (4.0×10^{-5} mol/L) versus pH values. SDS: (1) 0, (2) 8.0×10^{-3}, and (3) 6.0×10^{-2} mol/L.

In conclusion, morin is an effective antioxidant substance from natural plants and vegetables. However, its application is partly limited by its low solubility in aqueous solution. In this paper, SDS micelles with a hydrophobic core and with rich diversification in structure and microenvironment are used to solubilize morin. The electronic absorption and fluorescence emission spectra studies show that morin can be located in the SDS micelles with the B-ring part (dashed-frame part in **Figure 1**), which deviates by 38.98° from planarity in the molecule. The location of the morin in the SDS micelle leads to the increase of the planarity and the extension of π conjugation of the whole morin molecule. In the SDS spherical micelle, morin mainly exists in the form of monomer, whereas in the rodlike micelle, morin mainly exists in the form of dimer due to its more compact structure and less solubilization space. The embedment of the 2′,4′-dihydroxyl group linked on the B-ring into a more hydrophobic environment makes the oxidant peak potential become higher accompanied with decreasing peak currents, but the solubilization does not change the redox electrode reaction process, which directly reflects the antioxidant

capability of morin. Morin can be located in the palisade of the SDS micelles, and the binding of the morin to the SDS micelle is a spontaneous ($\Delta G < 0$) and exothermic process ($\Delta H < 0$). The small value of ΔH (15.03 kJ/mol) shows that the interaction force driving the binding of the morin to the SDS micelles is the weak intermolecular force.

LITERATURE CITED

(1) Hertog, M. G. L.; Hollman, P. C. H.; Van de Putte, B. Content of potentially anticarcinogenic flavonoids of tea infusions, wines, and fruit juices. *J. Agric. Food Chem.* **1993**, *41*, 1242−1246.

(2) Heller, W.; Forkman, G. Biosynthesis of flavonoids. In *The Flavonoids: Advances in Research since 1996*; Harbonne, J. B., Ed.; Chapman and Hall: London, U.K., 1996; pp 499−535.

(3) Hertog, M. G. L.; Hollman, P. C. H.; Van de Putte, B. Content of potentially anticarcinogenic flavonoids of 28 vegetables and 9 fruits commonly consumed in The Netherlands. *J. Agric. Food Chem.* **1992**, *40*, 2379−2383.

(4) Gamache, P.; Ryan, E.; Acworth, I. N. Analysis of phenolic and flavonoids compounds in juice beverages using high-performance liquid chromatography with coulometric array detection. *J. Chromatogr*. **1993**, *635*, 143−150.

(5) Achilli, G.; Cellerino, G. P.; Gamache, P. H.; D'Eril, G. V. M. Identification and determination of phenolic constituents in natural beverages and plant extracts by means of a coulometric electrode array system. *J. Chromatogr*. **1993**, *632*, 111−117.

(6) Lamson, S. W.; Brignall, M. S. Antioxidant and cancer. Part 3: quercetin, *Altern. Med. Rev.* **2000**, *5*, 196−208.

(7) Takahama, U. J. Suppression of lipid photoperoxidant by quercetin and its glycosides in spinach chloroplasts. *Photochem. Photobiol*. **1983**, *38*, 363−367.

(8) Cheng, I. F.; Breen, K. On the ability of four flavonoids, baiciein, luteolin, naringenin, and quercetin, to suppress the Fenton reaction of the iron−ATP complex. *BioMetals* **2000**, *13*, 77−83.

(9) Bors, W.; Saran, M. Radical scavenging by flavonoid antioxidant. *Free Radical Res. Commun*. **1987**, *2*, 289−294.

(10) Solimani, R. The flavonols quercetin, rutin and morin in DNA solution: UV−vis dichroic (and mid-infrared) analysis explain the possible association between the biopolymer and a nucleophilic vegetable-dye. *Biochim. Biophys. Acta* **1997**, *1336*, 281−294.

(11) Makris, D. P.; Rossiter, J. T. Hydroxyl free radical-mediated oxidative degradation of quercetin and morin: a preliminary investigation. *J. Food Compos. Anal.* **2002**, *15*, 103−113.

(12) Gutierrez, A. C.; Gehlen, M. H. Time-resolved fluorescence spectroscopy of quercetin and morin complexes with Al^{3+}. *Spectrochim. Acta Part A* **2002**, *58*, 83−89.

(13) Song, Y.; Kang, J. W.; Wang, Z. H.; Lu, X. Q.; Gao, J. Z.; Wang, L. F. Study on the interaction between CuL_2 and morin with DNA. *J. Inorg. Biochem.* **2002**, *91*, 470−474.

(14) Fang, S. H.; Hou, Y. M.; Chang, W. C.; Hsiu, S. L.; Lee, C.; Pei, D.; Chiang, B. L. Morin sulfates/glucuronides exert anti-inflammatory activity on activated macrophages and decreased the incidence of septic shock. *Life Sci.* **2003**, *74*, 743−756.

(15) Song, Y. M.; Kang, J. W.; Zhou, J.; Wang, Z. H.; Lu, X. Q.; Wang, L. F.; Gao, J. Z. Study on the fluorescence spectra and electrochemical behavior of ZnL_2 and Morin with DNA. *Spectrochim. Acta Part A: Mol. Biomol. Spectrosc.* **2000**, *56*, 2491−2497.

(16) Kalynasundaram, K.; Thaomas, J. K. Environmental effects on vibronic band intensities in pyrene monomer fluorescence and their application in studies of micellar systems. *J. Am Chem. Soc*. **1977**, *99*, 2039−2044.

(17) Guo, R.; Yu, W. L.; Zhang, X. H. Effect of VC on the phase behavior of surfactant systen. *Acta Phys-Chim. Sin*. **2000**, *16*, 325−330.

(18) Zsila, F.; Bikadi, Z.; Simonyi, M. Probing the binding of the flavonoid, quercetin to human serum albumin by circular dichroism, electronic absorption spectroscopy and molecular modelling methods. *Biochem. Pharmacol.* **2003**, *65*, 447−456.

(19) Liu, R. T.; Yang, J. G.; Wu, X.; Hua, S.; Sun, C. X. Interaction of morin with CTMAB: aggregation and location in micellar. *Spectrochim. Acta Part A* **2001**, *57*, 2561−2566.

(20) Liu, W. Y.; Guo, R.; Guo, X. Isomerization of malachite green in CTAB/*n*-$C_nH_{2n+1}OH/H_2O$ mixed micelles. *J. Dispersion Sci. Technol.* **2003**, *24* (2), 219−228.

(21) Guo, R.; Liu, W. Y.; Fan, G. K. Interaction of malachite green with CTAB micelles. *Acta Phys-Chim. Sin*. **2001**, *17* (12), 1062.

(22) Guardia, M. D. L.; Cardells, E. P.; Sancenon, J.; Carrion, J. L.; Pramauro, E. Fluorimetric determination of binding constant between micelles and chemical systems. *Microchem. J.* **1991**, *44*, 193−200.

(23) Song, G. P.; Guo, R.; Yang, Y. F. Fluorimetric determination of binding constant and distribution coefficients of ethanol in the SDS micelles system. *J. Yangzhou Technol. Coll. (Nat. Sci.)* **1992**, *12*, 42−47.

(24) Xue, Q. *The Spectrum Methods in the Structure Study of the Macromolecule*; High Education Press: Beijing, China, 1995; p 26.

(25) Sengupta, P. K.; Kasha, M. Excited-state proton-transfer spectroscopy of 3-hydroxyflavone and quercetin. *Chem. Phys. Lett*. **1979**, *68*, 382−385.

(26) Falkovskaia, E.; Sengupta, P. K.; Kasha, M. Photophysical induction of dual fluorescence of quercetin and related hydroxyflavones upon intermolecular H bonding to solvent matrix. *Chem. Phys. Lett*. **1998**, *297*, 109−114.

(27) Zhu, Z. W.; Li, C.; Li, N. Q. Eletrochemical studies of quercetin interacting with DNA. *Microchem. J.* **2002**, *71*, 57−63.

(28) Rice-Evans, C. Plant polyphenols: free radical scavengers or chain-breaking antioxidants. *Biochem. Soc. Symp*. **1995**, *61*, 103−116.

Received for review December 22, 2004. Revised manuscript received February 25, 2005. Accepted March 3, 2005. This work is supported by the National Natural Scientific Foundation of China (20233010).

JF047847P